CHANDRA
X-ray Center 60 Garden St., Cambridge Massachusetts 02138 USA

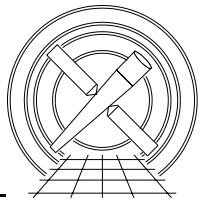

MEMORANDUM

Date: February 4, 2003
From: Richard J. Edgar, for the extended ACIS calibration team
Subject: Release of FEF files for CTI Corrected front-illuminated ACIS chips at –120 C
File: ~edgar/ACIS_FI_RMF/marple5_ACIS_FI_RMF/events_uncor/i1/fef_test/ReleaseNotes/release_notes.tex
Version: 1.9

---

1 Abstract

We present a new release of ACIS response products for the ACIS extended imaging array front-side devices (chips I0, I1, I2, I3, and S2). These products are a part of CALDB release 2.21, and are for use with the CXC implementation of the charge transfer inefficency (CTI) correction software in the new revision of `acis_process_events` released with `ciao` 2.3. They should be used with data taken at -120° C (which includes nearly all data taken since 2000 January 31).

These products were tested against data from the onboard external calibration source (ECS) taken in the spring of 2000, and against astrophysical sources (mainly the supernova remnant 1E0102-72.3) from calendar year 2000.

The gains and line widths are accurate at energies from 1.5 to 6 keV. The gains in nearly every case to 0.3% or better, and the line widths to better than an ADU.

There remain systematic residuals in our E0102 fits at low energies (0.5–1.2 keV). Gain shifts of approximately 0.5–1% are not uncommon, and there may be issues with the line widths and/or astrophysical assumptions that went into the analysis.

2 Caveats

Note that these response products have been tested against data collected during the first few months of operation at -120°C, 2000 February through 2000 April. We are still in the process of assessing gain drifts which may have occurred since the spring of calendar year 2000. As of this writing, we believe these effects are less than or of order 0.5% per year. At low energies (see the section below on E0102 testing) the effect seems to be smaller.

Gains are within 0.3% for nearly every tile, as determined by fits to the onboard external calibration source (ECS). This source has strong lines at just three energies: 1.47, 4.51, and 5.9 keV. At lower energies, the products were tested against the supernova remnant 1E0102-72.3, which has a relatively simple, soft, line-dominated spectrum. Some systematics remain in the residuals, which indicate gain errors of approximately 0.5–1.0% in some places on some chips. There may also be line with issues, and/or incorrect astrophysical assumptions in the model used in the fitting.

3 New Files and their Application

This document describes the following files, to be released as a part of the Chandra CALDB release 2.21:

These files are all found in directories under `$CALDB/data/chandra/acis/`.

- CTI-corrected FEFs:
  - `cpf/fefs/acisD2000-01-29fef_pha_ctiN0002.fits`
- Gain file to match the above FEFs:
  - `bcf/gain/acisD2000-01-29gain_ctiN0001.fits`
- Trap-map file for use with `acis_process_events` :
  - `bcf/cti/acisD2000-01-29ctiN0002.fits`

We will not discuss here other files released recently, such as non-CTI-corrected FEF files. The N0002 FEF file differs from the N0001 file released with CALDB 2.18 in November 2002 in the correction of a syntax error in the header. The practical effect is of order 1% in the wings of the lines for CTI corrected FI data, and is visible only in very high signal-to-noise data. The correction will allow this FEF file to be used to generate RMFs for non-CTI-corrected data as well, for those chips for which the CXC CTI correction is not available (*i.e.* S array chips other than S2).

These response products have been tested against data collected during the first few months of operation at -120°C, 2000 February through 2000 April. We are still in the process of assessing gain drifts which may have occurred since the spring of calendar year 2000. As of this writing, we believe these effects are less than or of order 0.5% per year.

4 Generating FI FEF files

In this section, we describe the generation of the new FI FEF files.

4.1 Brief description of MIT simulator and addCti.pro program

The MIT PI team (specifically Gregory Prigozhin) have developed a Monte-Carlo CCD simulator. There are two programs, intended to simulate front-illuminated (FI) and back-illuminated (BI) devices. They are described in SPIE papers linked from G. Prigozhin's home page

`http://space.mit.edu/~gyp/publications.html`.

The simulator programs described the performance of the devices as they were at the time of launch. Thus, the BI simulator includes both serial and parallel CTI, while the FI simulator does not include CTI, since it was immeasurably small at the time of the launch.

Unfortunately, during the first 60 days or so of the mission, substantial damage due to protons with energies of a few hundred keV occurred in the FI devices. The parallel CTI in the imaging arrays of the FI devices is now rather large. Flight operation techniques (hiding ACIS during radiation belt passages) has cut the rate of increase of the CTI to pre-launch predictions, but the damage has been done.

In order to assess the degree of CTI, to simulate it, and to some extent correct it, the MIT PI team (notably Bev Lamarr and Catherine Grant) with the collaboration of the PSU PI team (special thanks to Leisa Townsley and Pat Broos) developed trap map files, which are used by the CXC CTI corrector (which uses algorithms due to C. Grant and L. Townsley and others). These same files were incorporated into a post-processor for the MIT FI CCD simulator which degrades event pulse heights in a manner similar to the physical hardware, resulting in lower total pulse heights, poorer resolution, and grade changes, all very nearly as observed in the flight data.

It is this combination which we used to simulate the performance of the instrument for purposes of generating response matrix products. We ran the full-chip, diffuse illuminated simulations with the FI simulator program, and then degraded them using Bev LaMarr's addCti.pro program.

4.2 Factorization of Response

The BI FEF files released in August 2001 had seperately modeled response functions at 58 energies for each 32x32 pixel tile on node 1 of the S3 chip. An attempt to do a similar development for the FI chips failed, because the large parallel CTI makes the response change too rapidly across the chip for a reasonable set of starting functions to fit the response for all tiles. For this method to proceed, manual fitting of the spectrum at each energy for each tile would have been required.

Alexey Vikhlinin pointed out that the response can be factorized into two parts: one representing the response of the undamaged CCD chip, and the other representing the effects of CTI during the readout process.

Accordingly, we have obtained fit functions for these two factors, and we convolve them to obtain the FEF files for the full range of positions on the FI chips.

4.3 Non-CTI-degraded Response FEF

A functional form was developed which includes 5 Gaussians (to represent the peaks in the pulse height spectrum), a continuum consisting of a power law, and an additional broad Gaussian modified by error function (erf) and complimentary error function (erfc) cutoffs. It is intended that this function should represent the response of the undamaged CCD. Functions of this form were fit to the response from the MIT FI CCD simulator (without the CTI degradation of the addCti.pro program) for 89 energies ranging from 0.1 to 12.0 keV.

4.4 Derivation of the CTI Scatter Matrix

The CTI effects are encoded into a "CTI Scatter Matrix." The scatter matrix is substantially simpler than the full instrument response. It is continuous in energy, without edges or other jump discontinuities. We find it adequate to model this aspect of the instrument response with a function consisting of two summed Gaussians. These functions were fit by an automatic script, using the results of the addCti.pro program from the MIT PI team. This was done for 256x32 pixel regions (full node width in chipx, by 32 pixels in chipy) for every node of the FI chips in question (I0, I1, I2, I3, and S2).

4.5 Convolution

The CTI scatter matrix is then convolved in an approximate way with the undamaged response file as follows. Since the convolution of a Gaussian with another Gaussian is in turn a Gaussian function, neglecting the CTI effects in the power-law tail of the response, we obtain a function consisting of 12 Gaussian functions to represent the peaks in the response and the Gaussian part of the tail, plus the original, unconvolved, power-law tail fit function.

4.6 Gain Tweaking

Data from calibration observations of the on-board external calibration source (ECS) runs from a 3-month period in the spring of 2000 (from when the temperature was lowered to -120 C at the end of 2000 January) were coadded. The data were CTI corrected and split into the same tiles mentioned above by their chipx and chipy coordinates and PHA spectra were extracted. The strong lines (Al K-α at 1.49 keV; Ti K-α and K-β at 4.511 and 4.932 keV; and Mn K-α and K-β at 5.900 and 6.490) in the spectrum of the ECS were then fit using the trial response matrices. An xspec model consisting of 5 Gaussian lines with widths set to near zero, and energies set to the above values and then allowed to float, was used to fit these spectra. A matrix of errors in the centroids was prepared, and used to

E (keV)	Line	Node	Avg Err	Max Err	Median Err
1.487	Al_K$-\alpha$	I0c0	0.0757	0.5380	0.0673
1.487	Al_K$-\alpha$	I0c1	0.0441	0.3362	0.0673
1.487	Al_K$-\alpha$	I0c2	0.0463	0.3362	0.0673
1.487	Al_K$-\alpha$	I0c3	0.0504	0.4035	0.0673
4.510	Ti_K$-\alpha$	I0c0	0.0042	0.2217	0.0000
4.510	Ti_K$-\alpha$	I0c1	0.0152	0.2882	0.0222
4.510	Ti_K$-\alpha$	I0c2	0.0111	0.1996	0.0000
4.510	Ti_K$-\alpha$	I0c3	0.0042	0.1109	0.0000
5.898	Mn_K$-\alpha$	I0c0	0.0016	0.1356	0.0000
5.898	Mn_K$-\alpha$	I0c1	0.0016	0.1017	0.0000
5.898	Mn_K$-\alpha$	I0c2	0.0048	0.0848	0.0085
5.898	Mn_K$-\alpha$	I0c3	0.0021	0.1526	0.0000

Table 1: Summary Statistics for the I0 Energy Fit Parameters. Errors are in percent.

derive a smooth "gain tweak". This allows the gain of the physical amplifiers of the ACIS devices to be modeled empirically. The CTI scatter matrices were adjusted accordingly, re-convolved with the undamaged CCD response, and a new FEF file was produced.

This process was repeated as needed until all energies in the K-α lines in the ECS were fit to a precision of better then 0.3%.

5 Testing

5.1 External Calibration Source

Since the ECS data were used in the gain tweaking step above, we are already guaranteed that the gain matches at these energies to within the 0.3% energy specification. We include summary statistical tables of the fits we performed, and sample plots at the bottom, middle, and top of one node on each of the 5 FI chips.

The lack of any strong lines below 1.5 keV in the ECS spectrum forces us to look to astrophysical sources for verification of the FEFs at low energies.

E (keV)	Line	Node	Avg Err	Max Err	Median Err
1.487	Al_K−α	I1c0	0.0484	0.4035	0.0000
1.487	Al_K−α	I1c1	0.0546	0.6725	0.0000
1.487	Al_K−α	I1c2	0.0252	0.4707	0.0673
1.487	Al_K−α	I1c3	0.0462	0.3362	0.0673
4.510	Ti_K−α	I1c0	0.0139	0.1996	0.0111
4.510	Ti_K−α	I1c1	0.0014	0.1109	0.0000
4.510	Ti_K−α	I1c2	0.0014	0.1330	0.0222
4.510	Ti_K−α	I1c3	0.0049	0.1552	0.0000
5.898	Mn_K−α	I1c0	0.0037	0.1187	0.0000
5.898	Mn_K−α	I1c1	0.0011	0.0848	0.0000
5.898	Mn_K−α	I1c2	0.0027	0.1017	0.0000
5.898	Mn_K−α	I1c3	0.0000	0.0678	0.0000

Table 2: Summary Statistics for the I1 Energy Fit Parameters. Errors are in percent.

E (keV)	Line	Node	Avg Err	Max Err	Median Err
1.487	Al_K−α	I2c0	0.0589	0.4707	0.0336
1.487	Al_K−α	I2c1	0.0483	0.3362	0.0336
1.487	Al_K−α	I2c2	0.0504	0.3362	0.0673
1.487	Al_K−α	I2c3	0.0568	0.3362	0.0673
4.510	Ti_K−α	I2c0	0.0021	0.1552	0.0000
4.510	Ti_K−α	I2c1	0.0090	0.1109	0.0000
4.510	Ti_K−α	I2c2	0.0686	0.3326	0.0554
4.510	Ti_K−α	I2c3	0.0083	0.2439	0.0000
5.898	Mn_K−α	I2c0	0.0032	0.1187	0.0085
5.898	Mn_K−α	I2c1	0.0058	0.2035	0.0000
5.898	Mn_K−α	I2c2	0.0217	0.3052	0.0085
5.898	Mn_K−α	I2c3	0.0032	0.2035	0.0000

Table 3: Summary Statistics for the I2 Energy Fit Parameters. Errors are in percent.

E (keV)	Line	Node	Avg Err	Max Err	Median Err
1.487	Al_K−α	I3c0	0.0483	0.3362	0.0673
1.487	Al_K−α	I3c1	0.0357	0.4707	0.0673
1.487	Al_K−α	I3c2	0.0588	0.4707	0.0336
1.487	Al_K−α	I3c3	0.0525	0.2690	0.0673
4.510	Ti_K−α	I3c0	0.0111	0.1996	0.0000
4.510	Ti_K−α	I3c1	0.0007	0.1996	0.0000
4.510	Ti_K−α	I3c2	0.0049	0.2217	0.0000
4.510	Ti_K−α	I3c3	0.0166	0.1996	0.0000
5.898	Mn_K−α	I3c0	0.0042	0.1187	0.0085
5.898	Mn_K−α	I3c1	0.0244	0.3391	0.0000
5.898	Mn_K−α	I3c2	0.0021	0.1356	0.0000
5.898	Mn_K−α	I3c3	0.0069	0.1356	0.0085

Table 4: Summary Statistics for the I3 Energy Fit Parameters. Errors are in percent.

E (keV)	Line	Node	Avg Err	Max Err	Median Err
1.487	Al_K$-\alpha$	S2c0	0.0420	0.2018	0.0673
1.487	Al_K$-\alpha$	S2c1	0.0357	0.4707	0.0673
1.487	Al_K$-\alpha$	S2c2	0.0378	0.2690	0.0000
1.487	Al_K$-\alpha$	S2c3	0.0567	0.3362	0.0673
4.510	Ti_K$-\alpha$	S2c0	0.0021	0.4213	0.0111
4.510	Ti_K$-\alpha$	S2c1	0.0146	0.3769	0.0222
4.510	Ti_K$-\alpha$	S2c2	0.0152	0.1996	0.0111
4.510	Ti_K$-\alpha$	S2c3	0.0270	0.4656	0.0000
5.898	Mn_K$-\alpha$	S2c0	0.0080	0.2204	0.0085
5.898	Mn_K$-\alpha$	S2c1	0.0048	0.1696	0.0085
5.898	Mn_K$-\alpha$	S2c2	0.0318	0.4747	0.0254
5.898	Mn_K$-\alpha$	S2c3	0.0005	0.2543	0.0085

Table 5: Summary Statistics for the S2 Energy Fit Parameters. Errors are in percent.

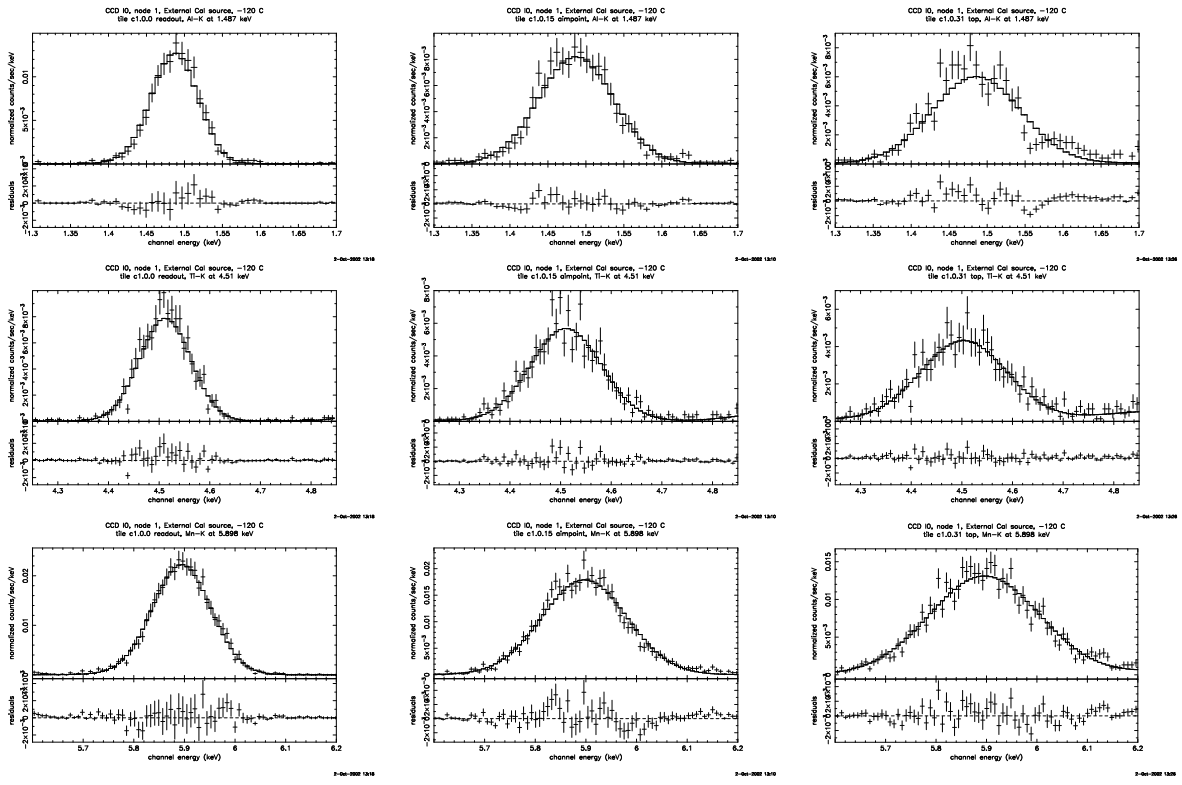

Figure 1: Fits to external calibration source lines: I0 c1, chipy=[1:32] (left), [481:512] (center), and [993:1024] (right). Lines are Al K–α (top), Ti K–α (middle), and Mn K–α (bottom).

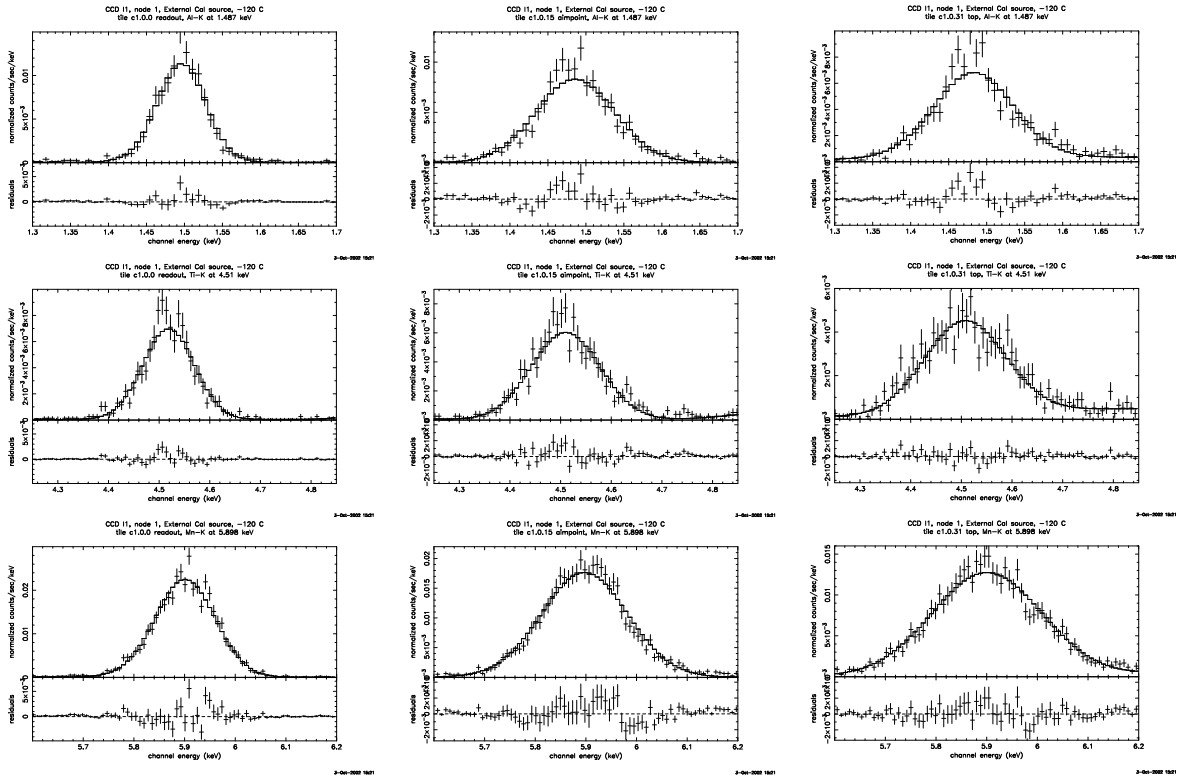

Figure 2: Same as Fig. 1 but for I1c1

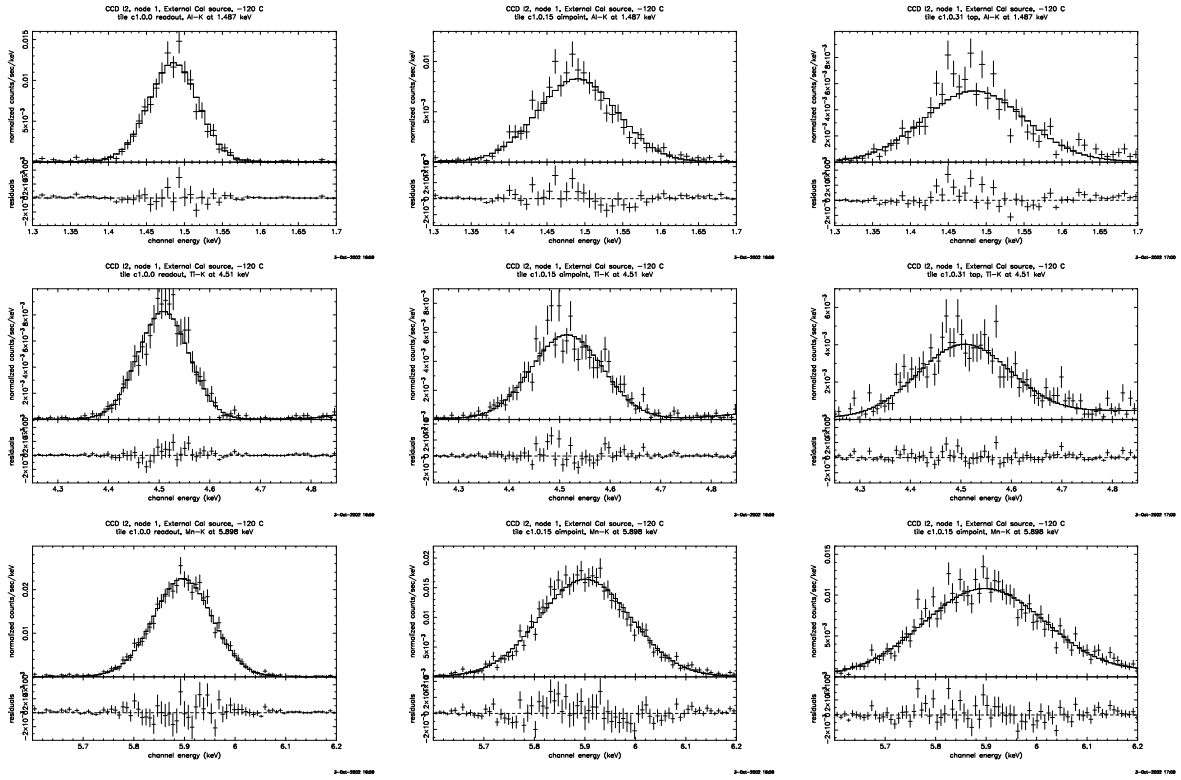

Figure 3: Same as Fig. 1 but for I2c1

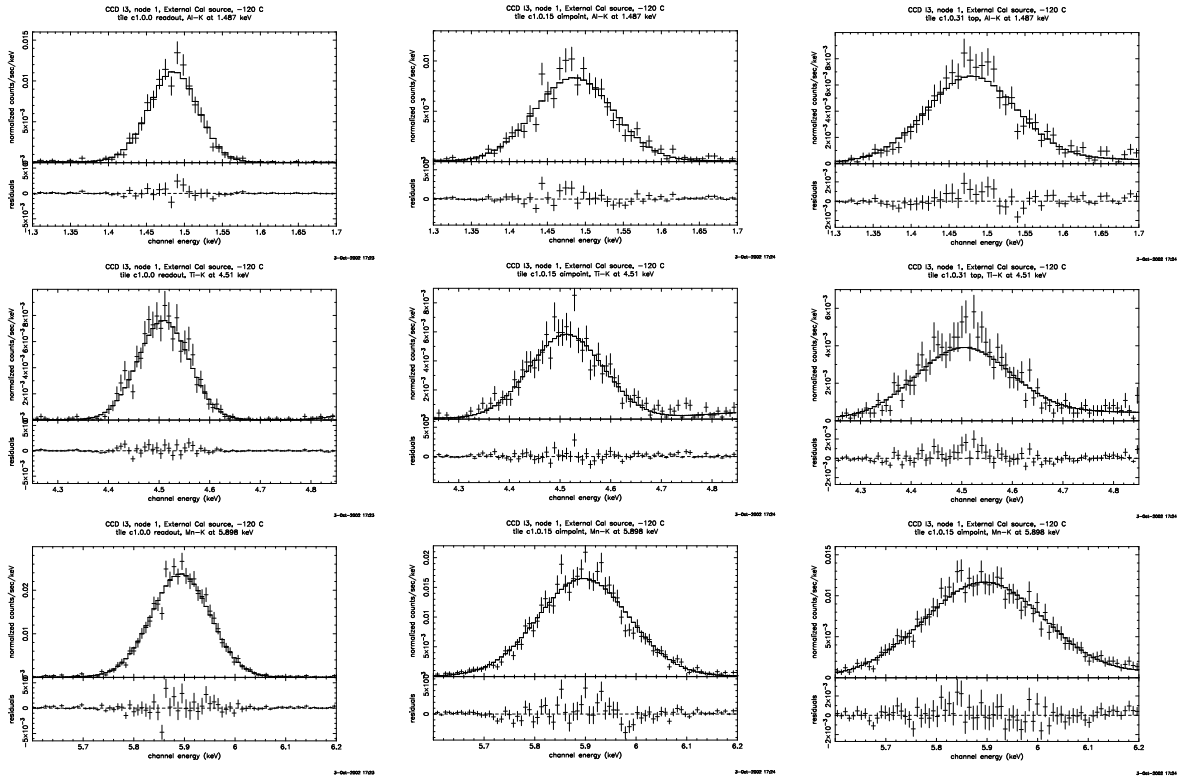

Figure 4: Same as Fig. 1 but for I3c1

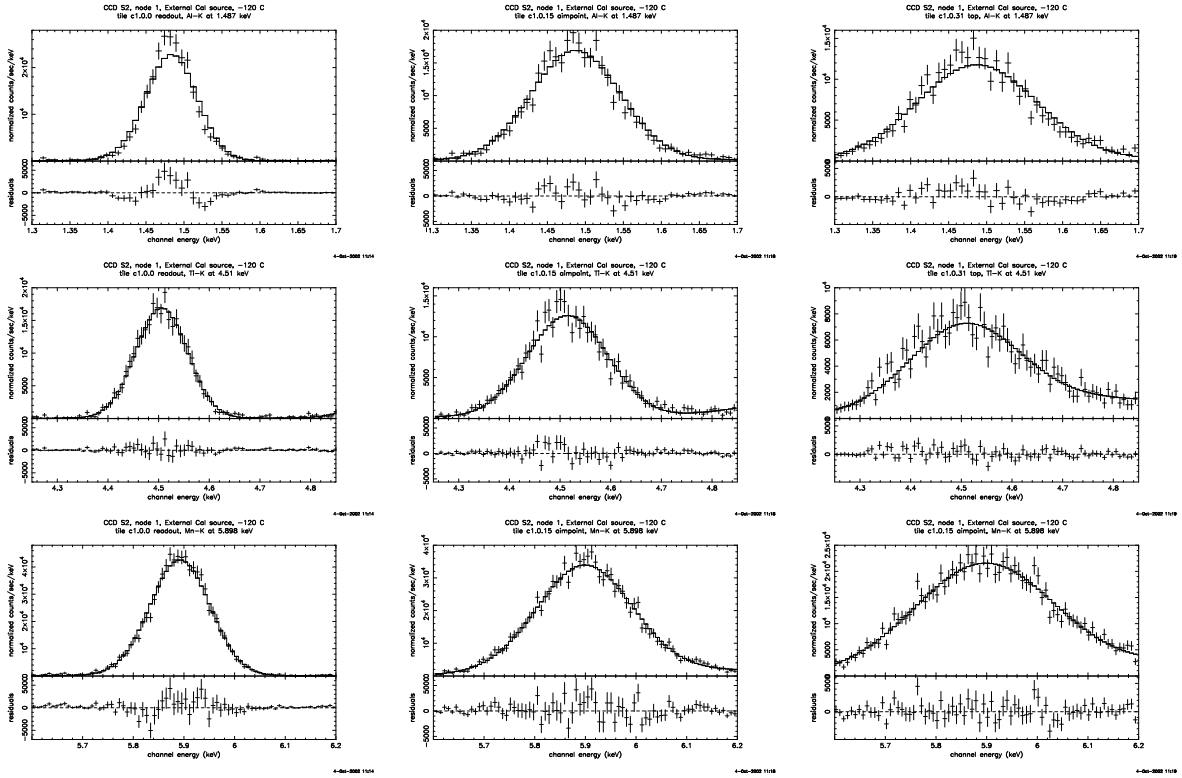

Figure 5: Same as Fig. 1 but for S2c1

5.2 E0102

The SMC supernova remnant (SNR) 1E0102-72.3 is in some ways a nearly ideal calibration source, which nicely complements the onboard external calibration source. The bright x-ray ring of this SNR is produced by a reverse shock propagating into the supernova ejecta, a gas composed almost exclusively of oxygen and neon, with no detectible iron. The spectrum consists of the helium-like triplet of lines from O VII and Ne IX, and the Lyman Alpha lines of hydrogenic O VIII and Ne X. At higher energies one also sees Mg and Si lines, at much lower levels. The absence of iron in the spectrum makes the neon lines at 0.9-1.02 keV usable for calibration purposes.

We have developed a spectral model in xspec for use in gain calibrations. It is based on line ratios taken from the HETG team's observation of this remnant (thanks to Kathy Flanagan and Amy Fredricks for the private communication). We have fixed the line ratios within the oxygen complex of lines, and within the neon complex of lines, but allowed the normalizations of the two complexes to vary independently. We have also allowed the line positions of the two complexes to vary independently, allowing two "gain" parameters, with the positions of the lines within each complex fixed relative to one another. There is, in addition, an absorbed thermal Bremsstrahlung model included. The line to continuum ratio for this source is quite large.

Table 6 shows results of fitting for gains in the oxygen (0.5–0.7 keV) and neon (0.9–1.1 keV) energy ranges. We list the best fit gain and the 90% confidence limits, as well as the date of the observation, the chipy tile used from the FEF file, and other data describing the observation. We have included data from all of calendar year 2000, since the data from the spring 2000 include only a few nodes of a few FI chips. The oxygen range gains are generally within about 0.5% of unity, while the neon range gains tend to be a bit more scattered.

Data from later epochs are included (Table 7) for completeness, though we did not adjust the current FEFs to match them. It can be seen from the fitted gains that there is not much time dependence at low energies. Work is underway to compare these FEFs to the external calibration source for epochs later than spring 2000 to verify the performance at higher energies as a function of time.

An examination of the figures (6–13) will show the character of the systematic residuals at low energies. In part these are due to the gain errors tabulated in Table 6, or line width issues. However, another effect that may contribute to the residuals may include an insufficiently flexible source model. The HETG-inspired model made certain assumptions about quantum efficiencies and astrophysics in order to derive line ratios we used. When the images in the various He-like line triplets overlap in the raw HETG data, an assumption must be made about the spatial structure of the SNR in each of the constituent lines.

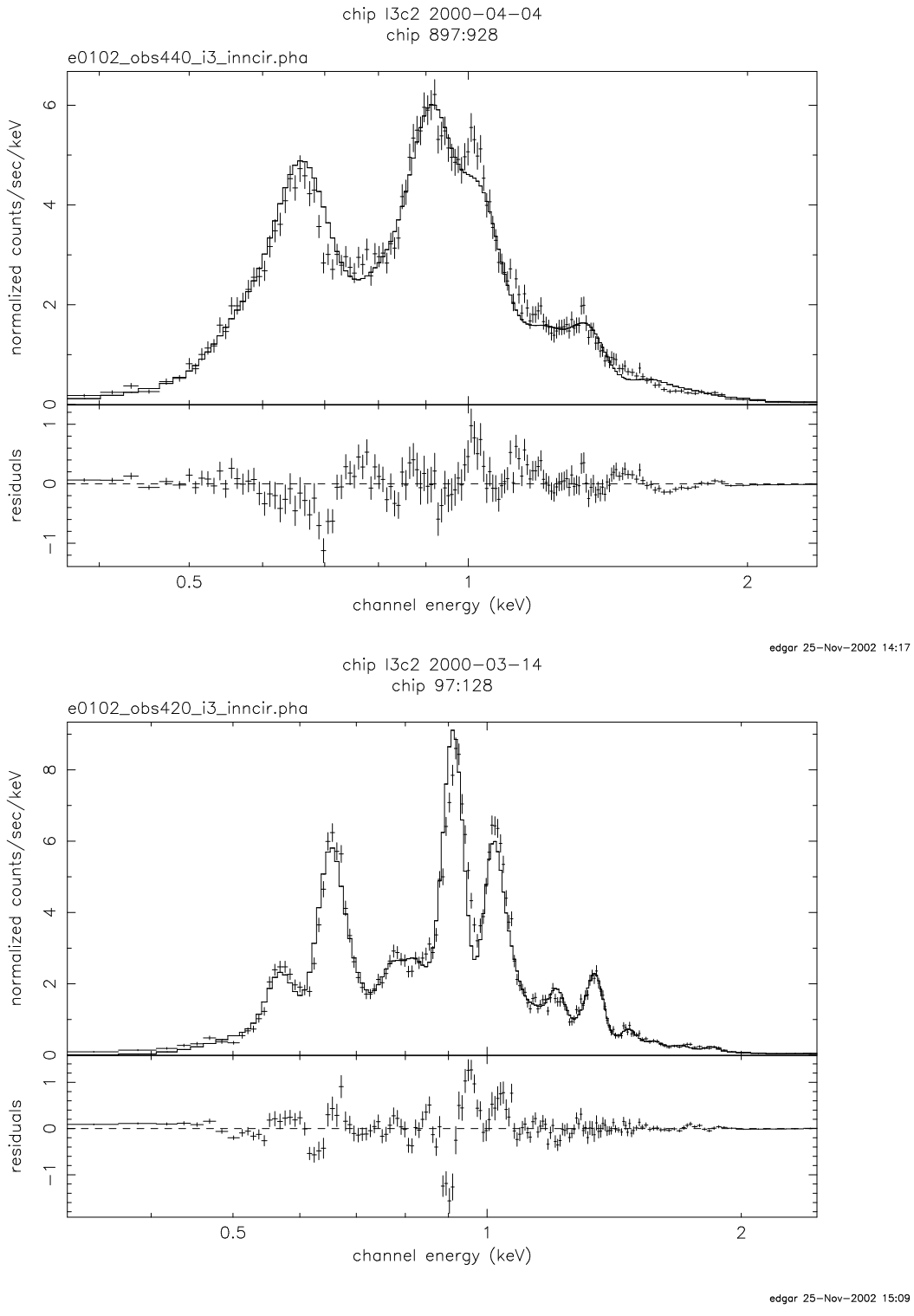

Figure 6: Best fit spectra of obsids 440 (top) and 420 (bottom) on I3c2. Obsid 440 is taken near the aimpoint (top of the chip), and so has large CTI effects. The dramatically better spectral resolution can be seen in Obsid 420, taken 7 arcmin off axis, near the chip readout.

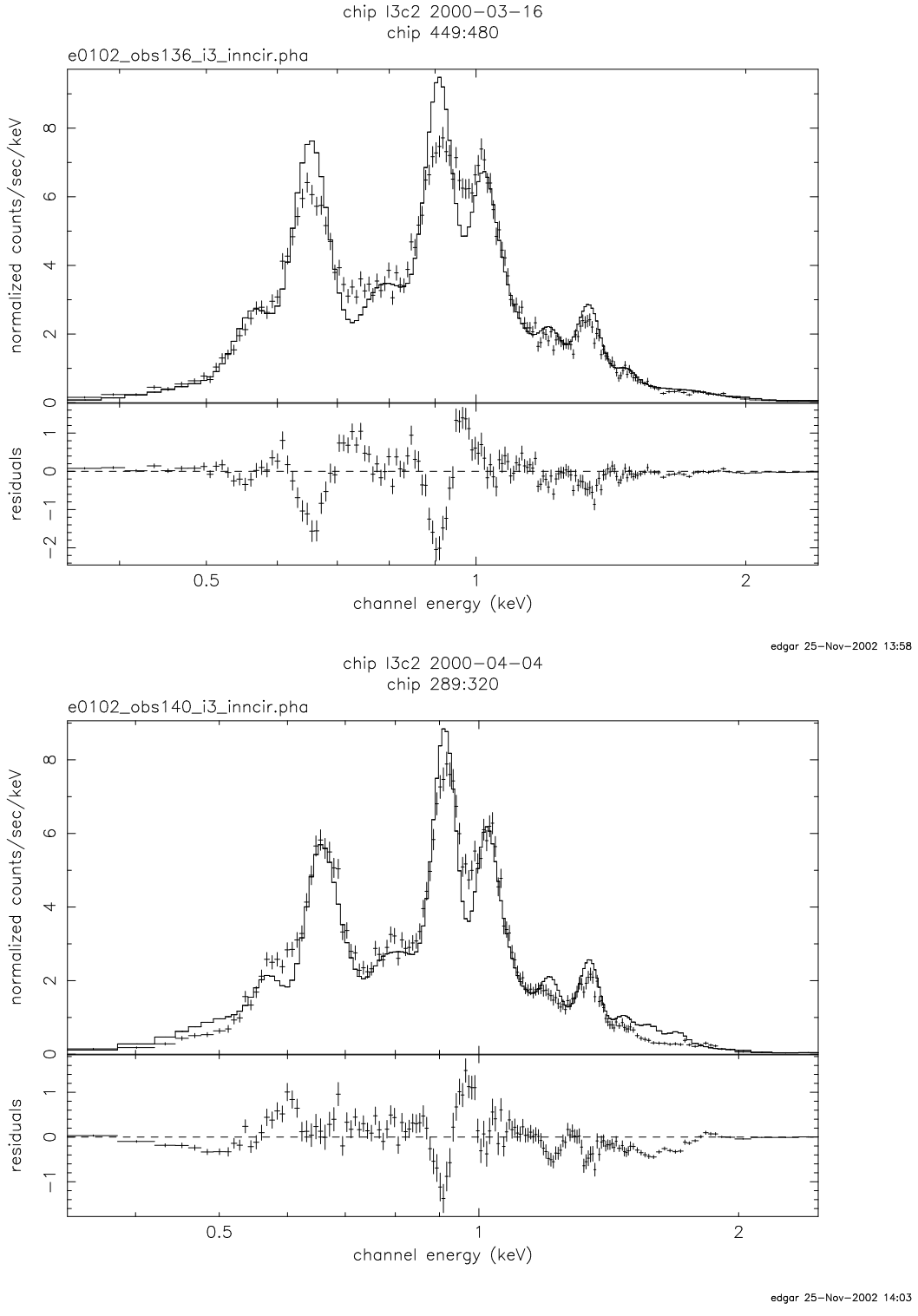

Figure 7: Best fit spectra of obsids 136 (top) and 140 (bottom) on I3c2.

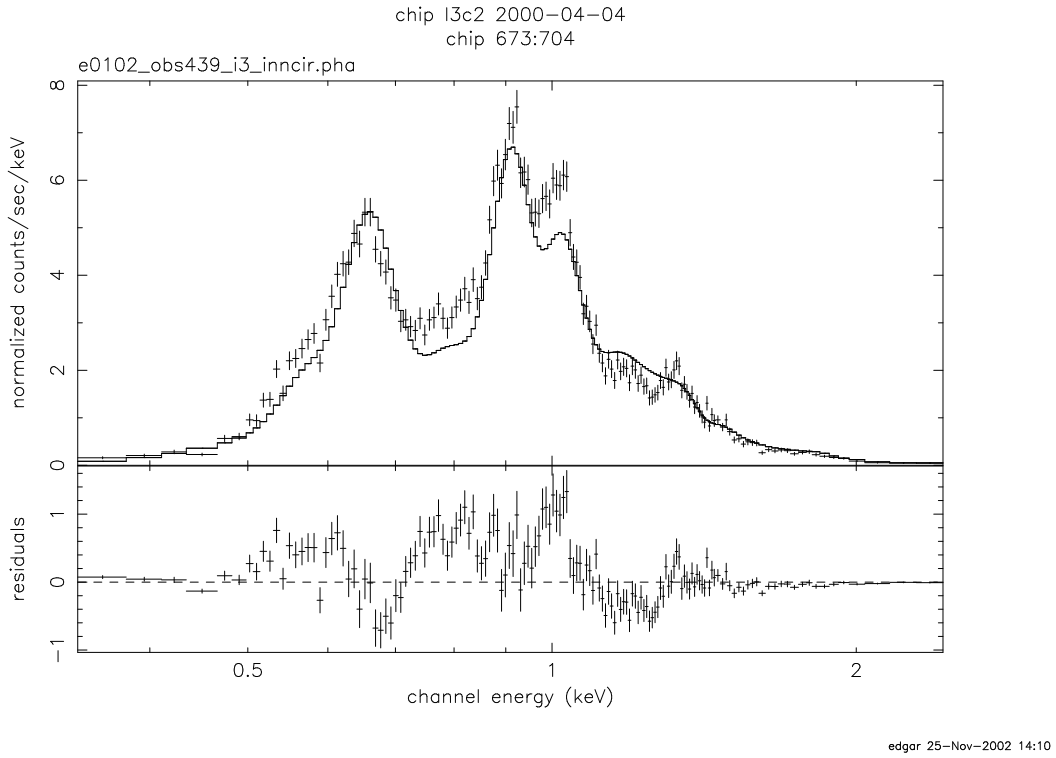

Figure 8: Best fit spectrum of obsids 439 on I3c2.

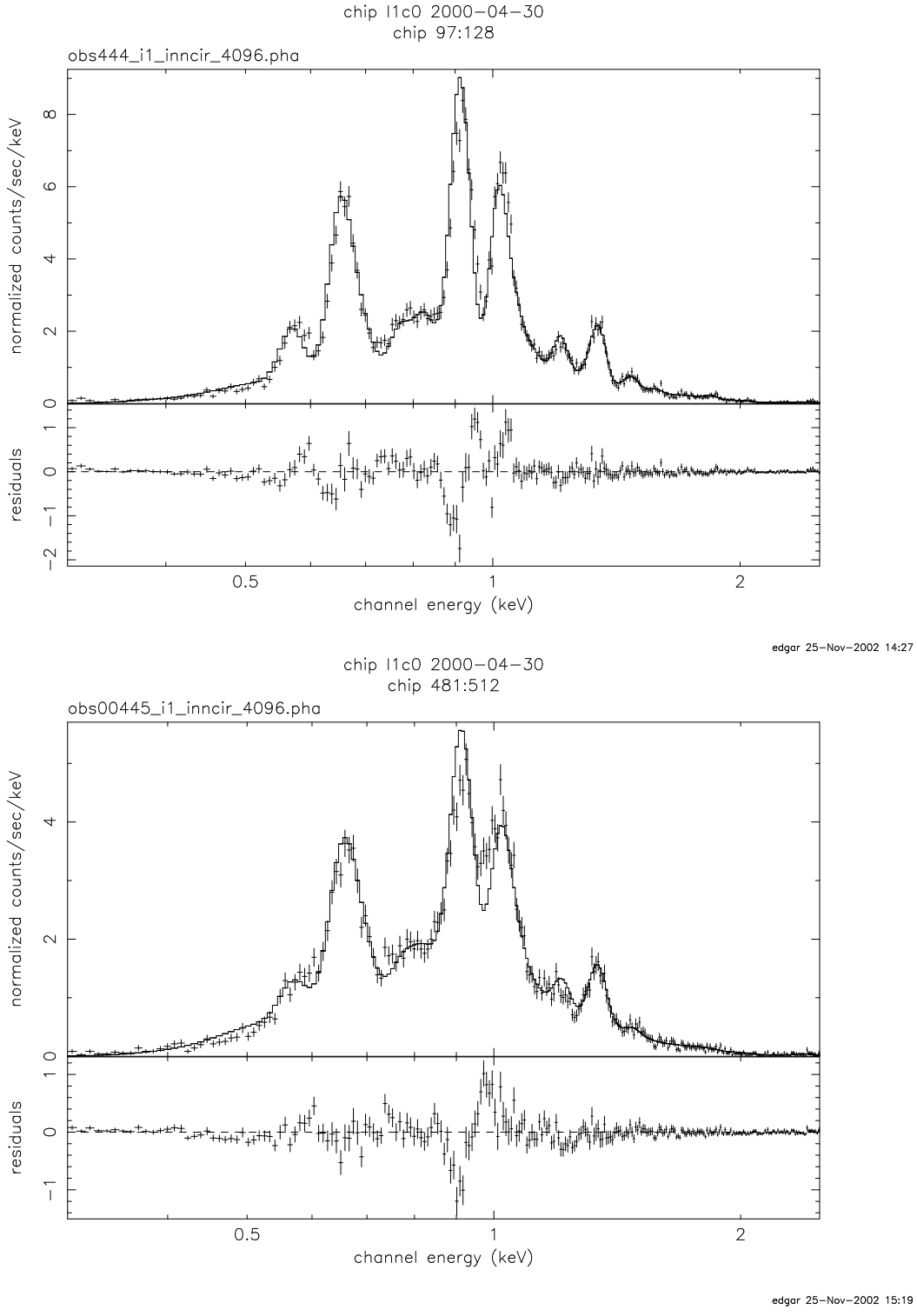

Figure 9: Best fit spectra of obsids 444 (top) and 445 (bottom) on I1c0.

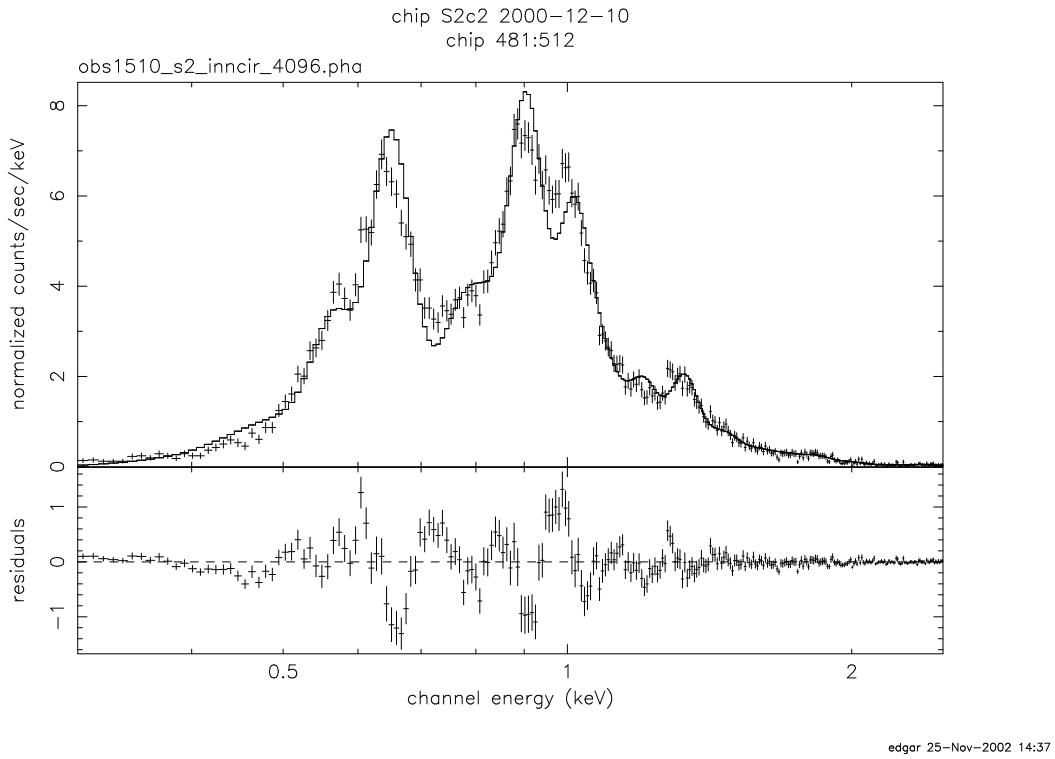

Figure 10: Best fit spectrum of obsids 1510 (top) on S2c2.

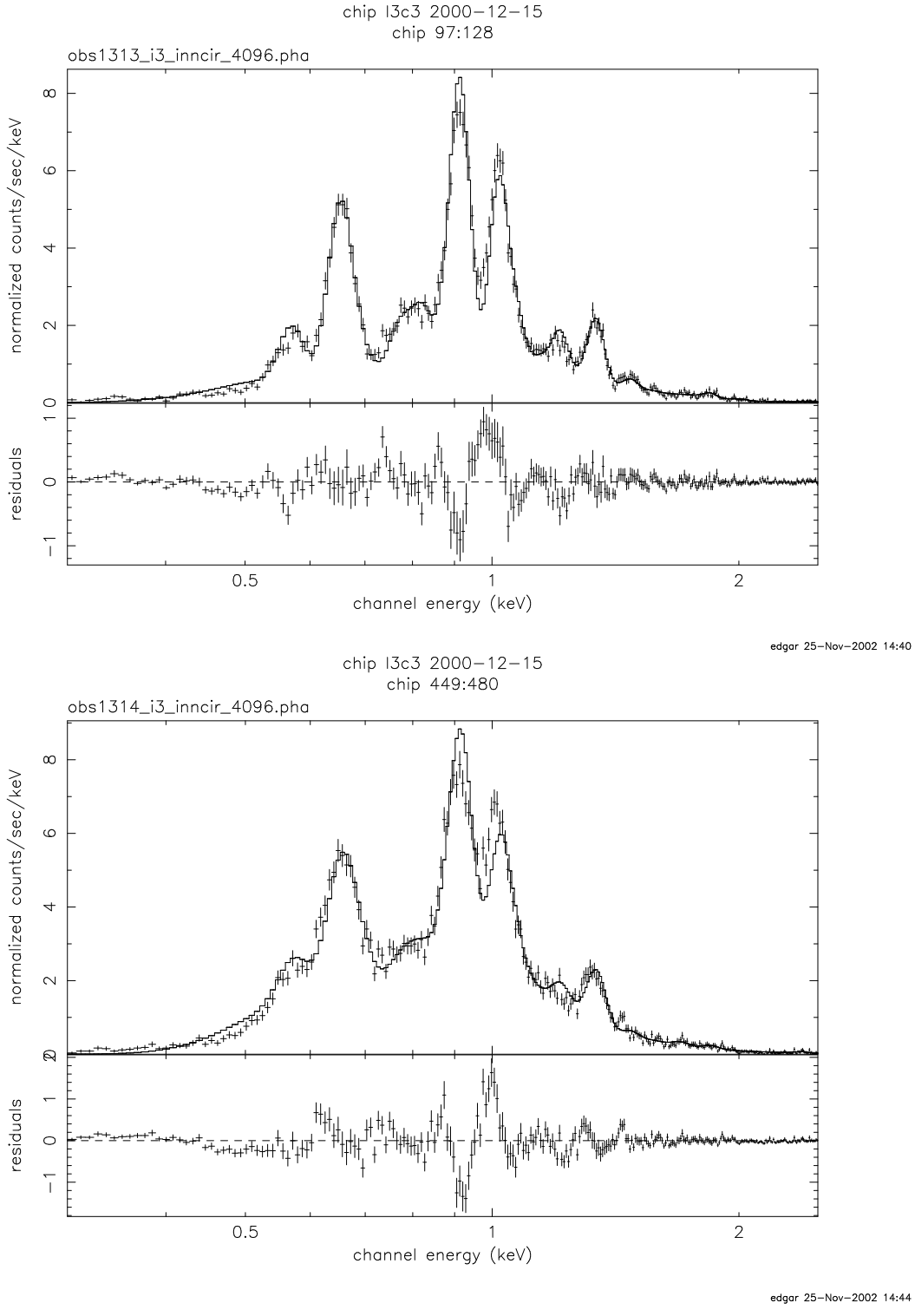

Figure 11: Best fit spectra of obsids 1313 (top) and 1314 (bottom) on I3c3.

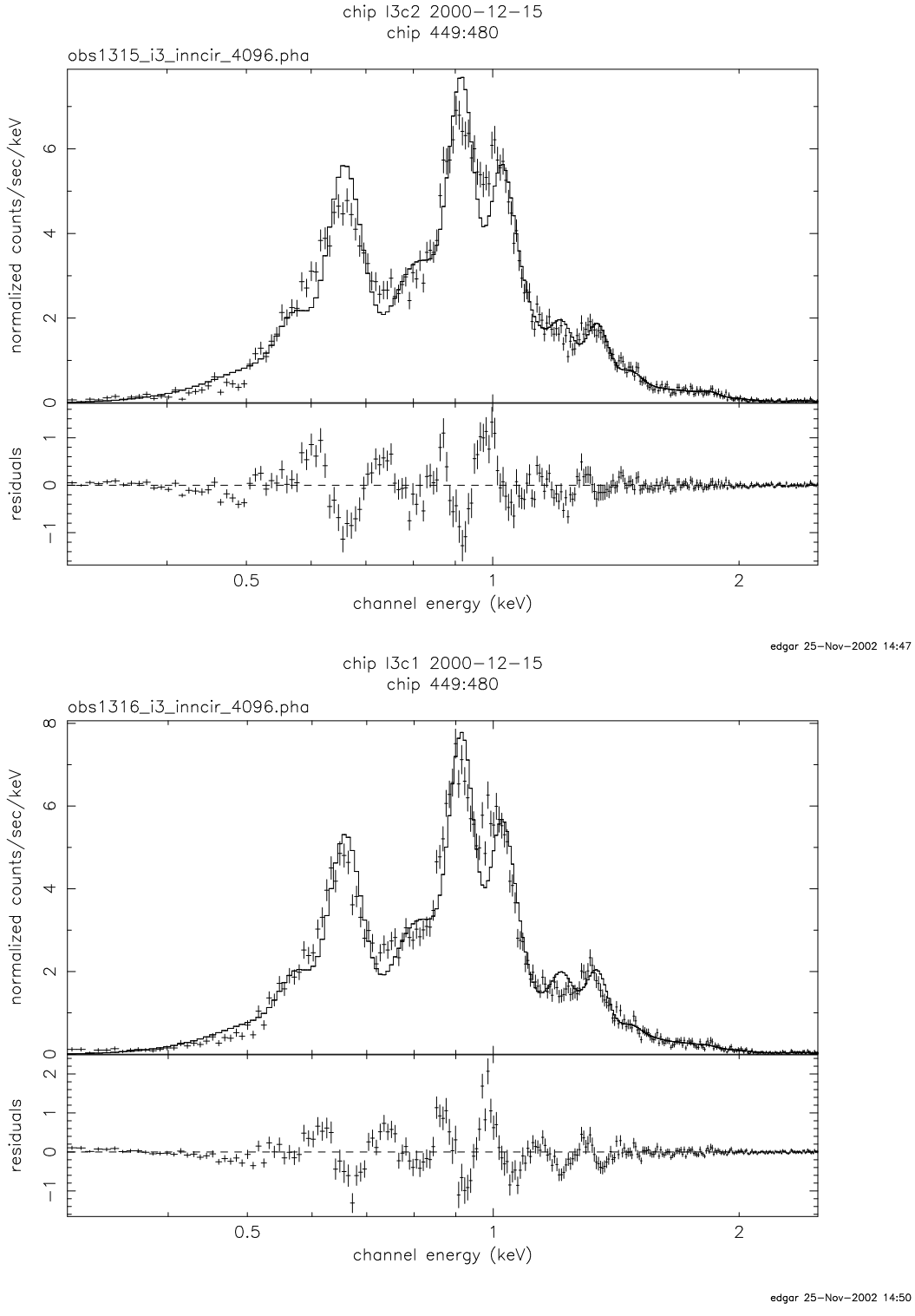

Figure 12: Best fit spectra of obsids 1315 (top) on I3c2, and 1316 (bottom) on I3c1.

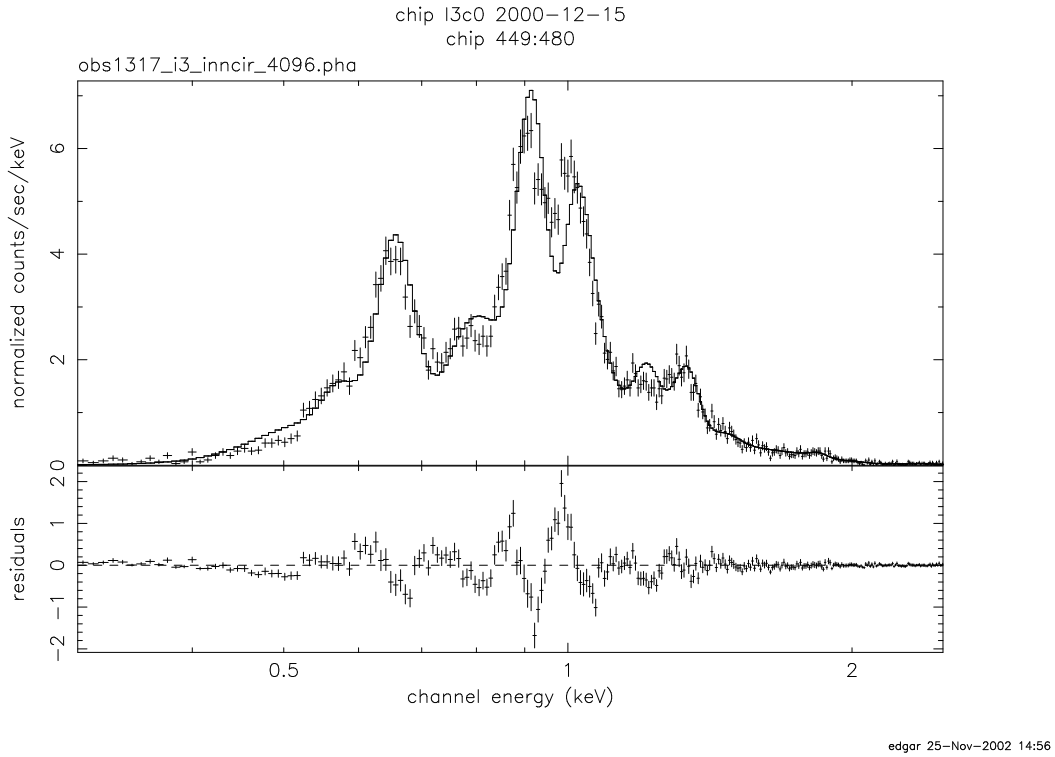

Figure 13: Best fit spectrum of obsids 1317 I3c0.

START_DATE	OBSID	chipy	O_gain	O_limits	Ne_gain	Ne_limits	CCD,node
2000−03−14 02:34:08.0	420	97:128	1.0020	1.0018:1.0030	1.0060	1.0041:1.0063	I3c2
2000−03−16 04:19:06.0	136	449:480	1.0048	1.0031:1.0066	0.9970	0.9969:0.9972	I3c2
2000−04−04 05:53:19.0	140	289:320	1.0072	1.0071:1.0075	0.9980	0.9971:0.9981	I3c2
2000−04−04 08:31:15.0	439	673:704	0.9977	0.9958:0.9982	0.9848	0.9835:0.9851	I3c2
2000−04−04 10:44:35.0	440	897:928	1.0005	1.0000:1.0017	0.9990	0.9983:0.9995	I3c2
2000−04−30 08:19:44.0	444	97:128	1.0085	1.0034:1.0097	1.0036	1.0031:1.0037	I1c0
2000−04−30 11:00:54.0	445	481:512	1.0000	0.9985:1.0006	0.9968	0.9968:0.9971	I1c0
2000−12−10 16:19:18.0	1510	481:512	0.9931	0.9930:0.3333	0.9865	0.9861:0.9875	S2c2
2000−12−15 11:33:58.0	1313	97:128	1.0047	1.0024:1.0065	0.9980	0.9969:0.9972	I3c3
2000−12−15 13:58:28.0	1314	449:480	1.0043	1.0027:1.0048	0.9970	0.9968:0.9973	I3c3
2000−12−15 16:06:58.0	1315	449:480	1.0048	1.0031:1.0064	0.9970	0.9970:0.9972	I3c2
2000−12−15 18:15:27.0	1316	449:480	0.9900	0.9888:0.9907	0.9865	0.9863:0.9870	I3c1
2000−12−15 20:23:58.0	1317	449:480	0.9847	0.9844:0.9865	0.9813	0.9806:0.9834	I3c0
2000−12−15 22:32:27.0	1527	545:576	0.9933	0.9931:0.9937	0.9914	0.9913:0.9916	I0c1
2000−12−16 00:40:57.0	1528	417:448	0.9931	0.9930:0.9936	0.9969	0.9968:0.9971	I1c1
2000−12−16 02:49:27.0	1529	513:544	0.9933	0.9931:0.9936	0.9969	0.9968:0.9970	I2c1

Table 6: Results of gain fitting for E0102 in calendar year 2000

START_DATE	OBSID	chipy	O_gain	O_limits	Ne_gain	Ne_limits	CCD,node
2001−06−05 06:33:56.0	1533	97:128	1.0050	1.0027:1.0096	0.9990	0.9980:1.0001	I3c3
2001−06−05 08:58:30.0	1534	481:512	0.9931	0.9931:0.9943	0.9865	0.9864:0.9870	I3c3
2001−06−05 11:16:14.0	1535	481:512	0.9903	0.9890:0.9906	0.9865	0.9860:0.9876	I3c2
2001−06−05 13:34:00.0	1536	481:512	0.9931	0.9930:0.9938	0.9865	0.9858:0.9874	I3c1
2001−06−05 15:53:22.0	1537	481:512	0.9913	0.9887:0.9919	0.9970	0.9968:0.9972	I3c0
2001−06−05 18:14:18.0	1542	513:544	0.9931	0.9931:0.9941	0.9865	0.9864:0.9875	I0c1
2001−06−05 20:33:36.0	1543	481:512	0.9931	0.9930:0.9935	0.9865	0.9864:0.9876	I1c1
2001−06−05 22:51:21.0	1544	513:544	0.9931	0.9930:0.9936	0.9970	0.9968:0.9972	I2c1
2001−06−06 10:59:06.0	1539	481:512	0.9931	0.9930:0.9940	0.9865	0.9861:0.9870	S2c2
2001−12−05 12:26:14.7	2835	97:128	1.0048	1.0031:1.0084	1.0045	1.0039:1.0045	I3c3
2001−12−05 14:44:44.7	2836	449:480	0.9903	0.9890:0.9911	0.9940	0.9938:0.9942	I3c3
2001−12−05 17:03:14.7	2837	449:480	0.9931	0.9931:0.9932	0.9865	0.9859:0.9878	I3c2
2001−12−05 19:21:44.7	2838	449:480	0.9931	0.9930:0.9938	0.9865	0.9861:0.9877	I3c1
2001−12−05 21:40:14.7	2839	449:480	0.9931	0.9931:0.9936	0.9865	0.9850:0.9879	I3c0
2001−12−05 23:58:44.7	2840	513:544	0.9931	0.9931:0.9935	0.9865	0.9863:0.9873	I0c1
2001−12−06 02:17:14.7	2841	449:480	0.9931	0.9931:0.9943	0.9865	0.9861:0.9889	I1c1
2001−12−06 04:35:44.7	2842	513:544	0.9905	0.9930:0.9935	0.9865	0.9863:0.9876	I2c1
2001−12−09 01:54:00.2	2847	481:512	0.9903	0.9890:0.9922	0.9865	0.9859:0.9870	S2c2
2002−06−21 02:08:00.0	2857	97:128	1.0050	1.0047:1.0062	0.9970	0.9969:0.9971	I3c3
2002−06−21 04:35:33.0	2858	481:512	0.9930	0.9931:0.9938	0.9865	0.9863:0.9873	I3c3
2002−06−21 06:55:43.0	2859	481:512	0.9931	0.9930:0.9936	0.9865	0.9864:0.9872	I3c2
2002−06−21 09:15:53.0	2860	481:512	0.9931	0.9930:0.9942	0.9865	0.9859:0.9873	I3c1
2002−06−21 11:36:03.0	2861	481:512	0.9932	0.9931:0.9937	0.9865	0.9862:0.9872	I3c0
2002−06−21 14:02:29.4	2862	513:544	0.9931	0.9931:0.9939	0.9865	0.9859:0.9872	I0c1
2002−06−21 16:16:23.0	2863	481:512	0.9934	0.9930:0.9936	0.9865	0.9862:0.9866	I1c1
2002−06−21 18:36:33.0	2864	513:544	1.0050	1.0037:1.0060	0.9970	0.9968:0.9972	I2c1
2002−06−22 08:49:03.0	2854	481:512	0.9931	0.9930:0.9937	0.9865	0.9865:0.9875	S2c2

Table 7: Results of gain fitting for E0102 in calendar year 2001 through June, 2002

	parameter	bestfit	min	max
obsid 1724 ciao 2.3 caldb 2.21				
	$N_{\rm H}$	2.66	2.57	2.75×10^{22}
	index	2.004	1.947	2.062
	norm	2.22	2.041	2.422×10^{-2}
obsid 1724 ciao 2.2.1, caldb 2.17				
	$N_{\rm H}$	2.69	2.60	2.78×10^{22}
	index	2.023	1.966	2.082
	norm	2.55	2.342	2.78×10^{-2}
obsid 1726 ciao 2.3 caldb 2.21				
	$N_{\rm H}$	2.52	2.43	2.61×10^{22}
	index	1.880	1.824	1.936
	norm	1.86	1.715	2.028×10^{-2}
obsid 1726 ciao 2.2.1, caldb 2.17				
	$N_{\rm H}$	2.46	2.37	2.54×10^{22}
	index	1.835	1.779	1.888
	norm	1.77	1.625	1.913×10^{-2}

Table 8: Results of fitting G21.5, with and without CTI correction

5.3 The Crab-like Supernova Remnant G21.5

The supernova remnant G21.5-0.9 is a center-filled synchrotron nebula, much like the Crab. The spectrum can be well fit by an absorbed powerlaw, though the powerlaw index depends on what part of the nebula is extracted. The absorbing column $N_{\rm H} = 2 - 3 \times 10^{22} {\rm cm}^{-2}$, which results in nearly all the photons below about 1.2 keV being absorbed.

For further details on this object, see Slane et al. 2000 ApJL, 533, L29, (2000).

We have fit two ACIS-I observations of G21.5 (obs 1724 & 1726) both observations were done on May 24, 2000. Obs 1724 is at an offset of -5.5 arcmin while obs 1726 is at an offset of -2.25 arcmin. Both were fit with an abosrbed powerlaw model in xspec. Both Observations were done at a temperature of -120 C. We fit them with the newly released response matrices, CTI corrector, ciao 2.3 and CALDB 2.21 (top panels in figs 14 and 15), and also using previously released data reduction and analysis tools, ciao 2.2.1 and CALDB 2.17. The results agree within errors.

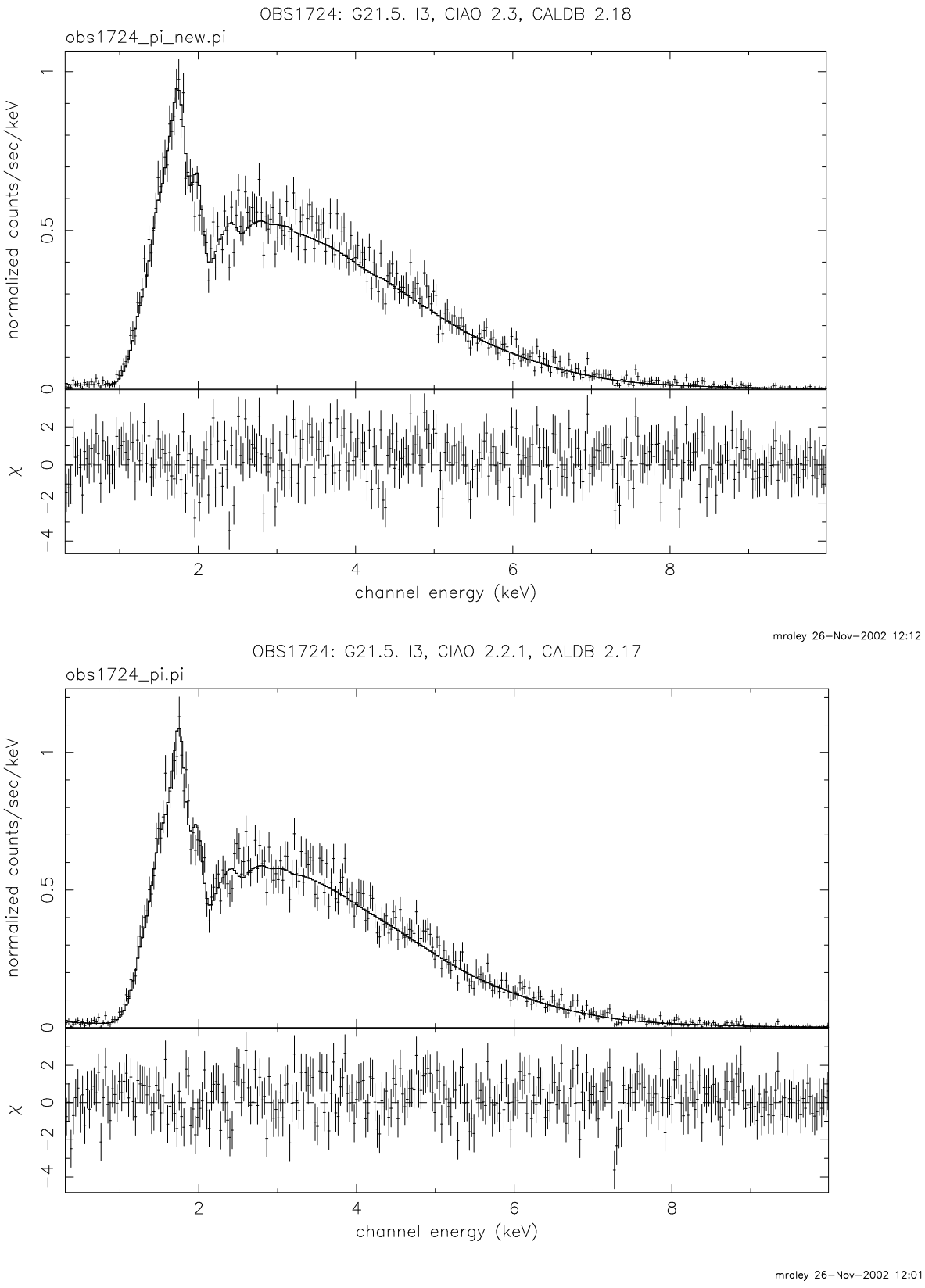

Figure 14: G21.5 spectra of obsid 1724, −5.5 arcmin off axis. Top: CTI-corrected, processed with ciao 2.3 and CALDB 2.21. Bottom: uncorrected, processed with ciao 2.2.1 and CALDB 2.17.

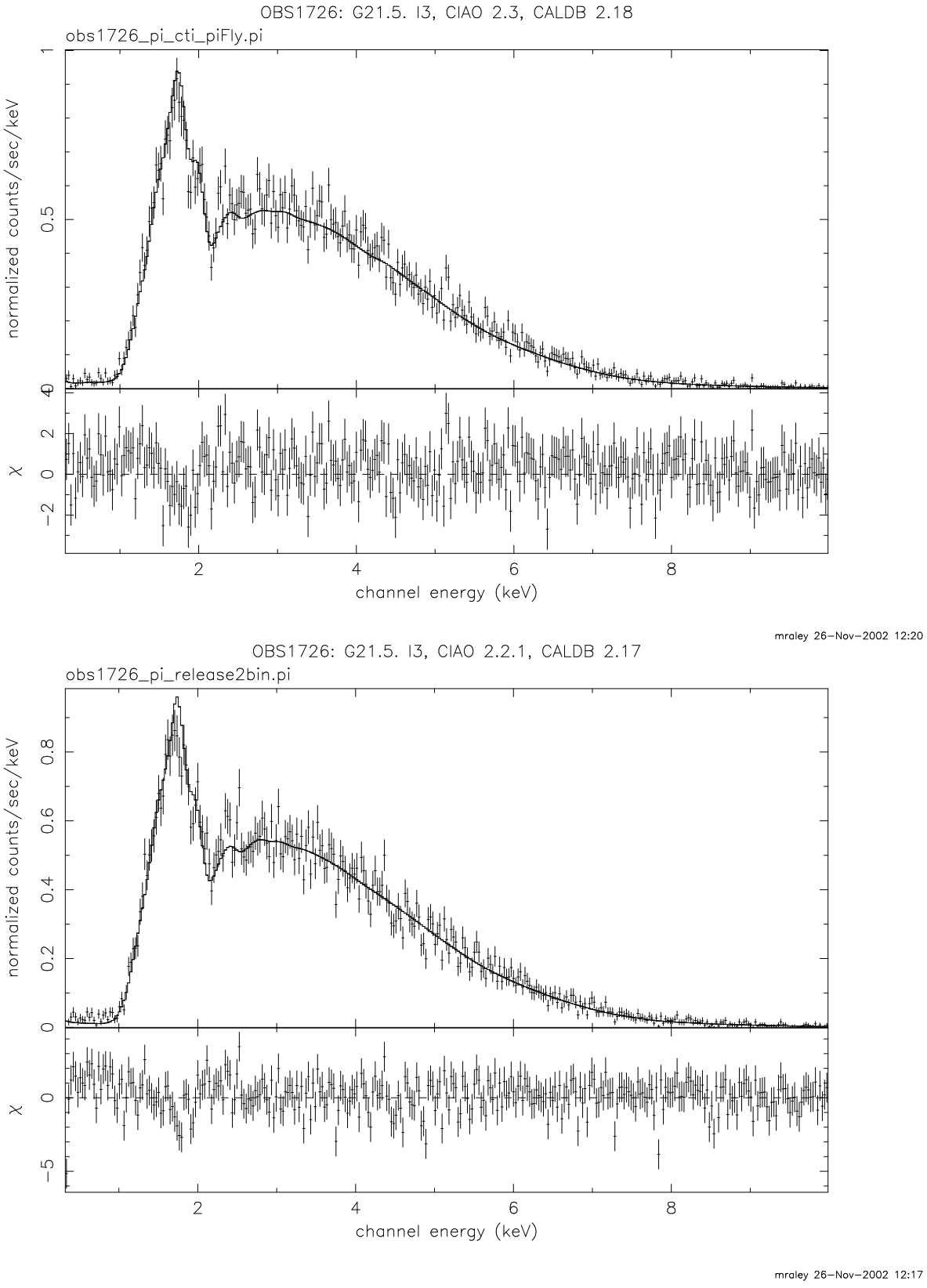

Figure 15: As for 15 but for obsid 1726, −2.25 arcmin off axis.

5.4 Distant Cluster cl0016+16

As another example of a spectral fit using CTI correction, Alexey Vikhlinin has analyzed an observation of a bright distant cluster, cl0016+16, using the CTI corrector, and using uncorrected data. The source region extends over 15 FEF tiles in two nodes of the I3 chip (nodes 2 and 3).

He fits a model of a single-temperature plasma, absorbed by a fixed (Galactic) column: wabs (mekal). The redshift is fixed at 0.541 (obtained from optical observations) and the column density is fixed at the Galactic value in this direction: 4.07×10^{20} cm^{-2}.

Using the CTI corrector, he obtains $kT = 10.09 \pm 0.49$ keV, abundances depleted by a factor of 0.288 ± 0.053, and a normalization factor (emission measure in native xspec units) of $(3.67 \pm 0.66) \times 10^{-3}$. Use of uncorrected PI responses gives $kT = 9.82 \pm 0.49$ keV, abundance $0.215 \pm .0492$, and a normalization of $(3.48 \pm 0.65) \times 10^{-3}$. So we see the fit parameters are the same within errors. In addition, the reduced chi squared statistic decreases from 1.29 (no CTI correction) to 0.88 (with CTI correction).

The PI response matrices used here are obtained dynamically from PHA FEF files, using the new feature of `mkrmf` released with ciao version 2.3 ("PI on the fly").

Note also a visible improvement in the energy resolution at the iron line near 4.5 keV. This is the Helium-like iron K–α line with rest energy $E = 6.7$ keV, redshifted by $z = 0.541$.

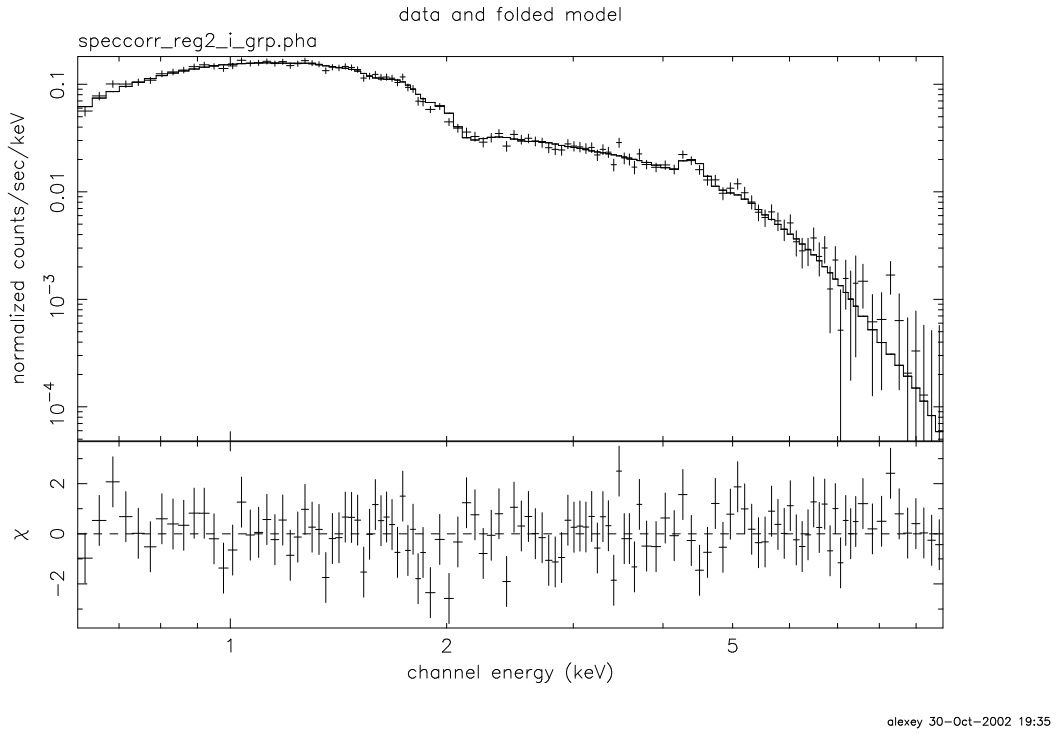

Figure 16: Best PI fit to distant cluster cl0016+16 with CTI-corrected FEFs. The region extends over 15 tiles and two nodes, I3c2 and I3c3. $\chi^2_\nu = 0.88$.

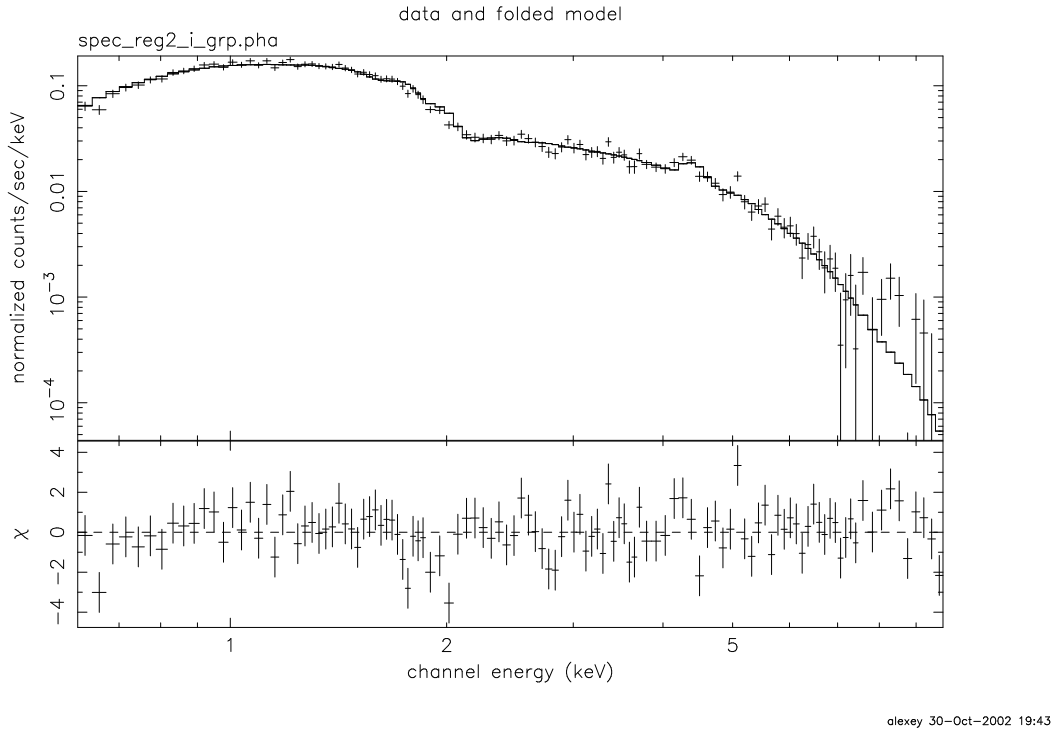

Figure 17: Best PI fit to distant cluster cl0016+16 with existing, released, non-CTI-corrected FEFs. $\chi^2_\nu = 1.29$.